Inorganic Chemistry

Article

pubs.acs.org/IC

Bond Characterization of a Unique Thiathiophthene Derivative: Combined Charge Density Study and X-ray Absorption Spectroscopy

Yu-Chun Chuang,[†,‡] Ya-Wen Li,[§] I-Jui Hsu,[§] Gene-Hsiang Lee,[∥] and Yu Wang*[,†]

[†]Department of Chemistry, National Taiwan University, Taipei 10617, Taiwan

[‡]National Synchrotron Radiation Research Center, Hsinchu 30076, Taiwan

[§]Department of Molecular Science and Engineering, National Taipei University of Technology, Taipei 10617, Taiwan

[∥]Instrumentation Center, College of Science, National Taiwan University, Taipei 10617, Taiwan

Supporting Information

ABSTRACT: Thiathiophthene (TTP), a planar molecule with two fused heterocyclic five-membered rings and an essentially linear S−S−S bond, is a molecule of great interest due to its unique chemical bondings. To elucidate the remarkable bonding nature, a combined experimental and theoretical study on the electron density distribution of 2,5-dimethyl-3,4-trimethylene-6a-TTP (**1**) is investigated based on a multipole model through high-resolution X-ray diffraction data experimentally and on the density functional calculations (DFT) theoretically. In addition, S K-edge X-ray absorption spectroscopy (XAS) is measured to verify the chemical bonding concerning the sulfur atoms. The molecule can be firmly described as 10π electron with aromatic character among the eight atoms, S_3C_5, of the two fused five-membered rings plus three-center four-electron σ character along the S−S−S bond. Such bonding description is verified with the calculated XAS spectrum, where the pre-edge absorption for transitions from S 1s to π^* and σ^* are located. The three-center four-electron S−S−S σ bond makes the terminal S atoms richer in electron density than the central one.

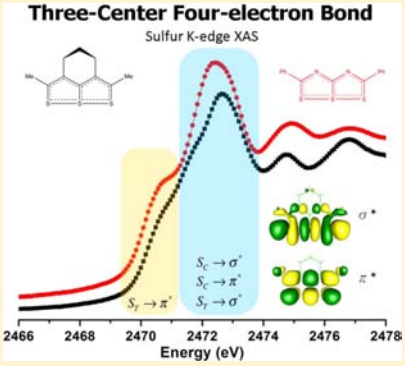

INTRODUCTION

Redox cleavage and/or formation of the S−S bond plays an important role in many chemical and biological processes.[1−4] Formation of a disulfide bond is known between cystine[5] residues in peptide chains, which is important in the folding process as well as the stability of many proteins. In addition, sulfur is also unique in its diversity of formal oxidation states and various coordination sites, for example, in compounds S_8, S_7NH, SF_6, $S(NR)_2$, $S(NR)_3$, SO_2, and K_2SO_4 etc. The chemical bonding concerning S has long been in debate[6,7] and drawn great attention in the literature. To avoid the violation of the octet rule in the valence shell, the argument of d-orbital involvement or hypervalency was raised. However, *molecular orbital* calculations indicate that inclusion of the d orbitals is simply used for the polarization function.[8−12] Thus, the electron density around S is apparently more diffused than second-row elements. The concept of a combination of resonance structures[11] including the ionic bonds to satisfy the octet rule yielded hypervalency. However, it was indicated strongly in a recent study of $S(NR)_x$ and K_2SO_4[13−15] that such concept is unnecessary. An alternative three-center four-electron (3c-4e) model was proposed[16−18] where two bonding electrons are distributed among three atoms and two additional electrons are located only on two terminal atoms, essentially of nonbonding character. Thus, the electron density around the terminal atom should be richer than that of the central one. The formal bond order is typically around 0.5; the corresponding bond distance is ∼0.18 Å longer than that with a bond order of 1.0.[19]

Because of such interesting bonding character, charge density studies have been applied to quite a few S-related compounds,[13−15,20,21] including the thiathiophthene (TTP) derivatives.[22−26] There are many TTP derivatives: some are symmetric with equal S−S bonds when the substituents are at the 2,5-positions;[23,25,26] others are asymmetric with a long and a short S−S bond when the substituents are at 2,4-positions.[22,24−26] The title compound, 2,5-dimethyl-3,4-trimethylene-6a-TTP, belongs to a symmetric one. It was indicated[27,28] that the Lewis resonance structures of TTP could be represented as in Figure 1, where the structure was described as a 10π electron[27] aromatic system[29,30] plus a 3c-4e σ bond along S−S−S. The deformation density of two TTP derivatives, one symmetric, 2,5-dimethyl-TTP, and the other asymmetric, 2,4-diphenyl-TTP, was investigated.[22−26] The S−S bond lengths of these compounds are all longer than the corresponding S−S single bond. The aim of this study is to establish the bond characterization on the title molecule through a combined experimental and theoretical charge density distribution as well as sulfur K-edge X-ray absorption spectroscopy (XAS).

Received: April 26, 2013
Published: September 10, 2013

   dx.doi.org/10.1021/ic4010455 | *Inorg. Chem.* 2013, 52, 10958−10967

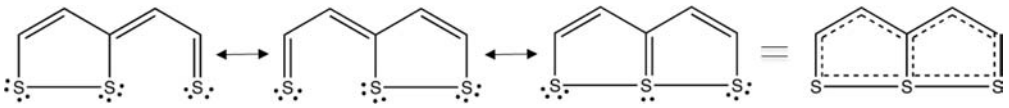

Figure 1. Lewis resonance structures of thiathiophthene (TTP).

EXPERIMENTAL SECTION

X-ray Diffraction Data Collection. A single crystal of suitable size was chosen to mount on a goniometer head in an arbitrary orientation. The crystal was cooled from room temperature to 100 K over a period of 1.5 h using an Oxford Cryosystem; software COLLECT[31] was used to calculate and optimize the goniometer and detector angular positions during data acquisition. Data were collected using ω-oscillation scans of 0.5° on a KappaCCD diffractometer. A total of 4983 images in 22 scan sets were measured over 184 h. Low-angle (1−27.5° in θ) and high-angle (20−50°) data were collected with an exposure time of 50 and 500 s/deg, respectively; the resolution of the data is up to 1.078 Å^{-1}. Images were integrated, and precise unit cell parameters were determined by postrefinement of the reflections using software EvalCCD.[32] Absorption corrections based on the measured crystal faces are applied using the program SADABS[33] without g-factor correction, while data are merged with the program SORTAV.[34] Crystallographic data of 100 and 300 K are deposited as CCDC-897210 and CCDC-942259 in the Cambridge Crystallographic Data Centre (CCDC) and can be accessed via www.ccdc.cam.ac.uk/data_request/cif.

Multipole Model Refinement. Structural parameters (atomic positions and displacement parameters) were first obtained by refining the high-order data [$\sin(\theta)/\lambda$ > 0.6 Å^{-1}]; then the multipole coefficients were refined using all data. Structural parameters obtained in the high-order refinement were fixed during refinement of the multipole parameters. Three models (Clementi−Roetti wave functions, relativistic Dirac−Fock wave functions, and STO atomic relativistic wave functions) were tried during refinement; final results were basically the same. The report here is based on Clementi−Roetti wave functions.[35] All atomic scattering factors were taken from the neutral atoms, with f' and f'' calculated using the program FPRIME.[36] Multipole expansion was up to hexadecapole for the S atom, up to octapole for the C atom, and up to dipole for the H atom. n_l values were (4, 4, 6, 8) and (2, 2, 3) for the S and C atoms, respectively. Hydrogen positional and thermal parameters were fixed during multipole refinement with a C−H distance of 1.08 Å. κ and κ' on the radial exponent were refined in the multipole refinement. Pseudo-C_s symmetry was imposed on the multipole coefficients of the molecule, where the internal coordinates were defined as shown in Figure S1, Supporting Information. The atomic parameter and multipole coefficients of atoms at the pseudomirror plane, S(2), C(3), and C(7), were constrained such that only P(0,0), P(1,1+), P(1,1−), P(2,0), P(2,2+), P(2,2−), P(3,1+), P(3,1−), P(3,3+), P(3,3−), P(4,0), P(4,2+), P(4,2−), P(4,4+), and P(4,4−) were allowed to be refined. Due to the different chemical environment, the κ and κ' parameters of the central S(2) and terminal S(1) and S(3) were refined separately.

DFT Calculation. The electron density of DFT calculation was obtained based on the experimental geometry using Gaussian03.[37] The B3LYP functional was used, and 6-31G+(d,p) basis set was used for all atoms. Topological analysis was performed using the program XAIM.[38] DENPROP[39] was used for visualization of the Laplacian distribution.

Sulfur K-Edge X-ray Absorption Measurements. Sulfur K-edge X-ray absorption experiments were performed at the BL16A beamline at the National Synchrotron Radiation Research Center (NSRRC), Hsinchu, Taiwan. Samples were ground and dispersed as thin as possible on Mylar tape to avoid the possibility of fluorescence saturation and self-absorption. Spectra were measured as fluorescence excitation spectra utilizing an ionization chamber as a Lytle detector, and the sample chamber was filled with high-purity He gas to avoid air absorption. The photon energy was calibrated at 2472.02 eV with the peak at the first pre-edge of $Na_2S_2O_3{\cdot}H_2O$. Before calculating the simulated spectra, experimental data is first truncated at 2475 and 2476 eV for **1** and **2**; multipeak fitting is then applied using OriginPro 9.0.[40]

TD-DFT Calculation. TD-DFT calculations for S K-edge spectra were carried out with the ORCA package version 2.9.1.[41] The S K-edge calculation was performed according to the procedure reported by Neese[42] and Solomon.[43,44] The B3LYP exchange functional and def2-TZVP(-f) basis set were chosen for S, N, C, and H atoms in the calculation. The geometry of **1** and **2** was taken from diffraction data and then optimized with the same basis set and exchange functional. Calculations included 125 excited states; convergence tolerances for residual and energy were set as 2.5 × 10^{-7} and 2.5 × 10^{-7} hartree, respectively. The simulated S K-edge absorption spectrum is displayed in Figure S9, Supporting Information. In order to get the right range of energy with the experimental data, an energy shift of 40.2 and 40.1 eV for **1** and **2** was applied to the calculated spectra to account for omission of the atomic relaxation associated with the core excitation and errors associated with the functional. All transitions below 2475 eV are convoluted with a pseudo-Voigt function with a 1:1 ratio of Lorentzian to Gaussian and a half-width of 0.5 eV to account for experimental and core hole broadening.

RESULTS AND DISCUSSION

Structure Description of 2,5-Dimethyl-3,4-trimethylene-6a-TTP (1). Similar to the crystal structures of several symmetrical substituted TTP derivatives,[45] this molecule does have C_s symmetry in the middle which is perpendicular to the molecular plane passing through S(2), C(3), and C(7), with a nearly linear S(1)−S(2)−S(1A) chain with a S−S distance of 2.3341(8) Å and an angle of 177.14(4)° at room temperature. However, at 100 K, the mirror symmetry disappears due to a slight displacement of sulfur chain. The space group changes from $C2/m$ to $P2_1/n$. Nevertheless, it still contains nearly equal S−S bond distances, 2.3393(5) and 2.3274(5) Å, and a S(1)−S(2)−S(3) angle of 176.864(8)°. The molecule is basically planar with all non-hydrogen atoms located on the same plane, except the C(7) atom, which is away from the plane due to its sp^{3}configuration. The molecular structure of **1** is displayed with atomic labeling in Figure 2. Crystal data and selected bond distances are listed in Tables 1 and 2, respectively. Two

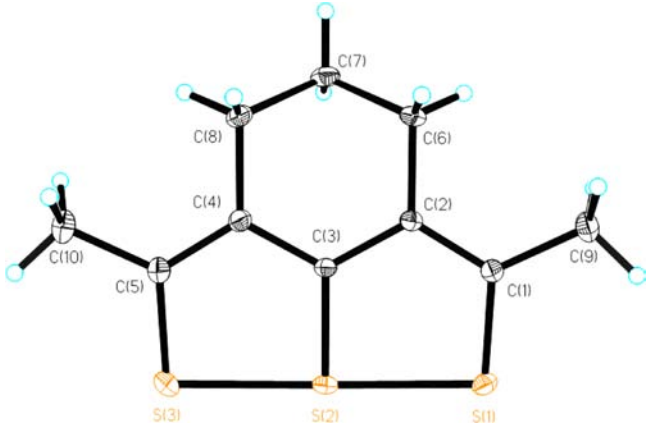

Figure 2. Molecular structure and atom labeling of 2,5-dimethyl-3,4-trimethylene-6a-TTP drawn with 50% probability ellipsoids at 100 K.

dx.doi.org/10.1021/ic4010455 | Inorg. Chem. 2013, 52, 10958−10967

Table 1. Crystallographic Data of 2,5-Dimethyl-3,4-trimethylene-6a-TTP

temp	100 K	300 K
formula	$C_{10}H_{12}S_3$	$C_{10}H_{12}S_3$
cryst syst	monoclinic	monoclinic
space group	$P2_1/n$	$C2/m$
a (Å)	8.1072(5)	14.033(3)
b (Å)	11.0499(6)	11.195(2)
c (Å)	11.4713(8)	8.210(2)
β (deg)	90.187(3)	124.26(3)
V (Å^3)	1027.6(4)	1065.8(4)
Z	4	4
abs coeff (mm^{-1})	0.669	0.645
cryst size	0.24 × 0.21 × 0.06	0.24 × 0.21 × 0.06
no. of reflns collected/unique/obsd	78584/8472/7135 [R(int) = 0.0543]	4340/999/744 [R(int) = 0.0377]
T_{max}/T_{min}	0.9610/0.8559	0.9623/0.8606
spherical atom refinement		
data/restraints/params	8472/0/166	999/0/91
goodness-of-fit on F^2	1.121	1.050
final R indices [$I > 2\sigma(I)$] (all data)	R_1 = 0.0277 (0.0377)	R_1 = 0.0331 (0.0501)
	wR_2 = 0.0671 (0.0719)	wR_2 = 0.0844 (0.0919)
largest diff. peak and hole	0.667 and −0.305 e·A^{-3}	0.156 and −0.247 e·A^{-3}
multipole model refinement		
data/restraints/params	6450/94[a]/266	
final R [$I > 3\sigma(I)$] (all data)	R_1 = 0.0176 (0.0369), wR_1 = 0.0191	R_1 = 0.0176 (0.0369), wR_1 = 0.0191
	R_2 = 0.0277 (0.0298), wR_2 = 0.0373	R_2 = 0.0277 (0.0298), wR_2 = 0.0373
goodness-of-fit S	0.9298	

[a]Pseudo-C_s symmetry is imposed on the multipole coefficients; $R_1 = \Sigma||F_o| - |F_c||/\Sigma|F_o|$; $wR_1(F) = [\Sigma w|F_o - F_c|^2/\Sigma w(F_o^2)]^{1/2}$; $wR_2(F^2) = [\Sigma w|F_o^2 - F_c^2|^2/\Sigma w(F_o^4)]^{1/2}$.

different S−C bond distances are found with the central S(2)−C(3) bond significantly longer than the terminal S(1)−C(1) and S(3)−C(5) bonds. Two different C−C bond distances of five-membered rings, 1.3821 and 1.4227 Å, are found which is consistent with the resonance structures presented in Figure 1. It is worth mentioning that the thermal parameter, U_{22}, of all S atoms, which is along the direction of S−S−S chain, is apparently larger than U_{11} and U_{33} at 300 K; however, such difference is not observed at 100 K. There is no short intermolecular contact found, the shortest one being 3.54 Å between the S atoms.

Multipole Model (MM). The molecular electron density in terms of the multipole model[46,47] is implemented using the program XD2006.[48] A pseudo-C_s geometry is imposed along S(2), C(3), and C(7) atoms with local coordinates defined as given in Figure S1, Supporting Information. The agreement indices of the MM model are significantly lower than the spherical model listed in Table 1; the corresponding residual maps are essentially featureless except along S−S bonds shown in Figure S2(a), Supporting Information; the jnk2RDA[49] residual density analysis yields a reasonable Gaussian distribution depicted in Figure S2(b), Supporting Information. The variation of F_o/F_c vs $\sin\theta/\lambda$ at the final stage is within ±1%, shown in Figure S3, Supporting Information. Thus, the MM model does represent a better model fit than the spherical one with the experimental data. The experimental deformation density, Laplacian distribution, and topological properties are derived based on this model.

Deformation Density and Laplacian of Electron Density. The deformation density map is the difference electron density between the molecule (MM) and the independent atomic model (IAM). The experimental and theoretical calculated deformation density maps at the molecular plane are depicted in Figure 3a and 3b, respectively. There is density accumulation along all C−C bonds as expected; similar accumulation is found along C−S bonds but in less density; the agreement between experiment and theory is very good in C−C bonds. The experimental deformation density is found near the terminal S nucleus not only toward the central S atom but also at the direction outward from the bisection of ∠C−S−S. However, there is only one density accumulation around the central S atom extended along the C−S direction; there is practically no accumulation from the theoretical one. Little accumulation is found along the S−S bonds. Significant difference between experiment and theory is found near the S nucleus, which makes different appearances along the S−S and S−C bonds; nevertheless, the general trend is similar. This may come from the difference in radial distributions between experiment and theory. The core contraction/expansion parameter[50] has been tried on sulfur atom; unfortunately it makes no improvement on the residual density around sulfur atoms.

An alternative way of looking at the bonding effect is from the Laplacian of the density, which is the second derivative of

Table 2. Topological Properties Associated with Selected Chemical Bonds[a]

	d_1 (Å)	ρ_b (e/Å^3)	$\nabla^2\rho_b$ (e/Å^5)	G_b[b] (H/Å^3)	H_b[c] (H/Å^3)	ε	δ(A,B)[d]
S(2)−S(1)	1.1372	0.607	3.21	0.44	−0.22	0.09	
2.3274(5)	1.1207	0.575	1.19	0.24	−0.15	0.19	0.81
S(2)−S(3)	1.1429	0.594	3.209	0.43	−0.21	0.09	
2.3393(5)	1.1259	0.561	1.27	0.24	−0.16	0.19	0.79
S(2)−C(3)	0.9204	1.326	−1.97	0.89	−1.03	0.18	
1.7500(7)	0.9070	1.386	−9.39	0.43	−1.09	0.22	1.24
S(1)−C(1)	0.8925	1.521	−5.61	0.91	−1.30	0.19	
1.7006(7)	0.8114	1.479	−11.42	0.59	−1.39	0.17	1.38
C(1)−C(2)	0.6996	2.299	−20.82	1.17	−2.63	0.18	
1.3822(7)	0.7077	2.157	−20.80	0.76	−2.21	0.28	1.43
C(2)−C(3)	0.7049	2.083	−16.79	1.07	−2.24	0.17	
1.4227(7)	0.6850	1.993	−18.34	0.62	−1.91	0.19	1.24

[a]First line is from the MM model and second line from DFT calculation. [b]Kinetic energy density. [c]Total energy density. [d]Bond delocalization index.

dx.doi.org/10.1021/ic4010455 | Inorg. Chem. 2013, 52, 10958−10967

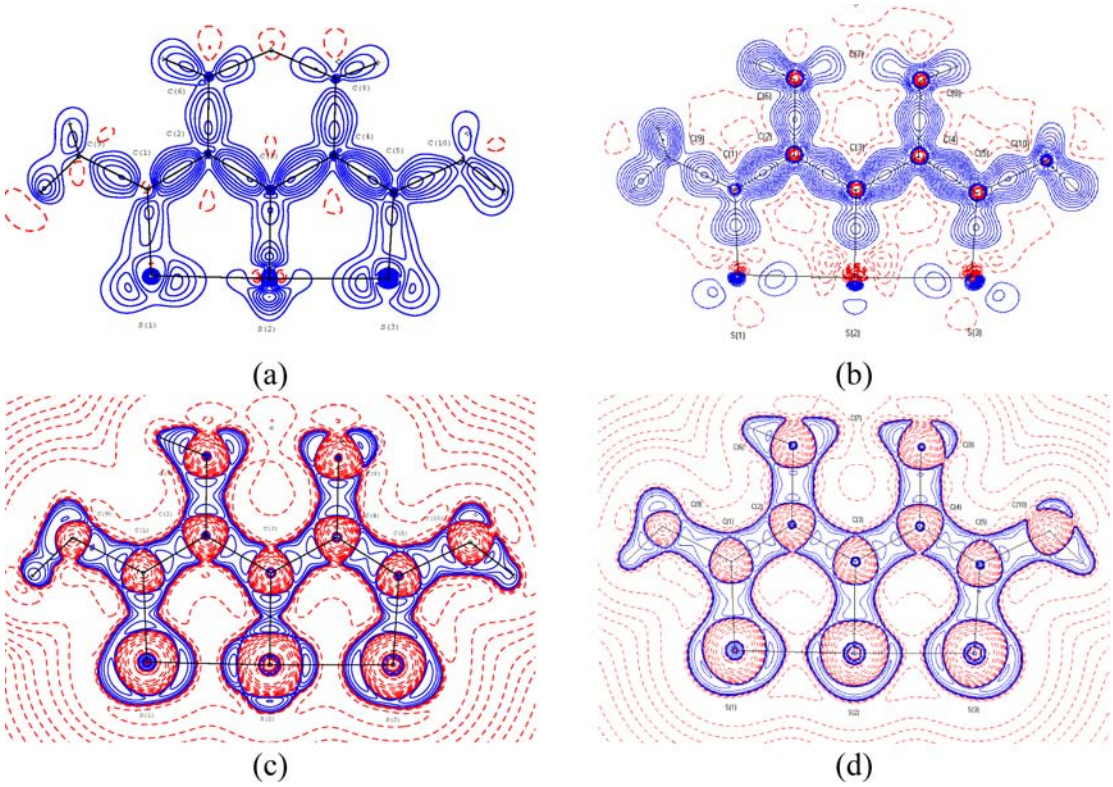

Figure 3. Deformation density maps at the molecular plane from (a) experiment and (b) theory. Contour interval $\pm 0.1 e/Å^3$; solid blue line, positive; dotted red line, negative. Laplacian of density at the same plane from (c) experiment and (d) theory. Contours are $\pm 2^m \times 10^n$ ($e/Å^5$), where m = 1, 2, 3 and n = −3, −2, −1, 0, 1, 2, 3, 4. Blue solid lines are negative, and the red dashed lines are positive.

the electron density. Local charge concentration (LCC) and local charge depletion (LCD) are shown as a negative and positive Laplacian, respectively. The Laplacian at the molecular plane derived from experiment and theory is displayed in Figure 3c and 3d, respectively. There are apparently three LCC around each C atom at the direction of the C−C or C−H bond, illustrating clearly the sp^2 hybrid type of C atom with such LCC from two bonded C atoms facing toward each other along the C−C bond. An obviously more complicated feature is found around the S atom: four distinct LCCs at the plane are observed around the central S(2) atom with maxima values located roughly at an angle of 90° from each other, but only three LCCs are observed at the plane around the terminal S(1) and S(3) atoms with two maxima located along the S−C and S−S bonds and the other at the bisection of ∠C−S−S, similar to those observed from the deformation density. Although the LCC from each bonded S atom is also facing toward each other, they are separated apart due to the long distance of the S−S bond. The agreement between experiment and theory is adequate. In order to view the surface around each S atom, 3D Laplacian isosurfaces around the central and terminal S atoms from experiment are depicted in Figure 4; those from theory are given in Figure S4, Supporting Information; the two isosurfaces are quite different from the one around the central, S being symmetric and shell like. Other than the LCC along each bonding direction, there are LCCs representing the lone pair regions around S atoms. In order to investigate further the shape of the Laplacian, an atomic graph is derived by taking the second derivative of the Laplacian; an atomic graph is a polyhedron around the nucleus to describe the shape of VSCC of the atom, where the vertices (V) and faces (F) are the critical point (3,−3) and (3,+3) of the Laplacian, respectively, and the

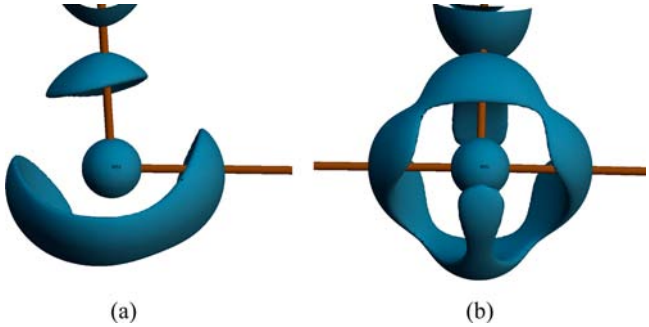

Figure 4. Experimental 3D Laplacian distribution around the (a) terminal S(1) and (b) central S(2) atom at an isosurface level of −8 and −6 $e/Å^5$, respectively; brown stick means S−S and S−C bonds.

edge (E) is the saddle point (3,−1) of the Laplacian. Such polyhedron should satisfy Euler's rule, V + F − E = 2. Vertices around the sulfur atoms are displayed in Figure 5, and a detailed description of the vertices of the polyhedron is listed in Table S1, Supporting Information: the central S atom gives a trigonal bipyramidal (TBP) shape, and the terminal S shows tetrahedral (T_d) shape with the vertices being 0.7 Å away from the nucleus. Therefore, in addition to the vertices along the S−S and S−C bond directions, two vertices are indicative of the lone pair region, which yields a TBP and T_d polyhedron around the central and terminal S atom, respectively.

Topological Properties. Topological analysis of charge density has been widely applied to the chemical bond characterization.[51] The topological properties associated with the bond critical point (BCP) could be used to classify the bond type, bond strength, etc. Such properties are listed in

dx.doi.org/10.1021/ic4010455 | Inorg. Chem. 2013, 52, 10958−10967

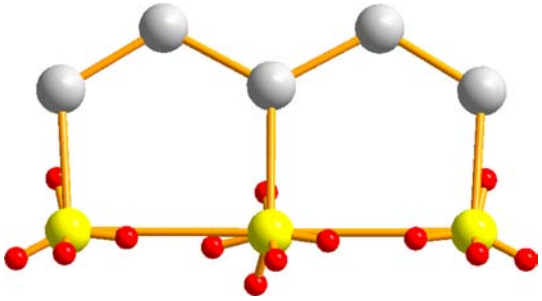

Figure 5. Atomic graph of sulfur atoms with the frame of TTP: gray and yellow balls, C and S, respectively; small red spheres, vertices, V (3,−3) around each S atom.

Table 2. All C−C bonds are typical shared interactions (covalent character) with the BCP located at the midpoint of the bond: the electron density at BCP, ρ_b, greater than 2 e Å^{-3}; large negative Laplacian, $\nabla^2\rho_b$, and a large negative value of total energy density, H_b being less than −2 HÅ^{-3}. However C(1)−C(2) is slightly stronger than C(2)−C(3) according to the distance, ρ_b, and H_b values. Two S−C bonds are also covalent with the BCP located 0.08 Å closer to the C atom; the location of BCP manifests the slight difference in electronegativity between S and C atoms. With ρ_b > 1.3 eÅ^{-3}, negative $\nabla^2\rho_b$, and H_b values of < −1.0 H Å^{-3}, again the terminal S(1)−C(1) is stronger than the central S(2)−C(3) bond. The S−C bonds in TTP are apparently stronger than the S−C bond of thiourea *S*,*S*-dioxide, with a ρ_b value of 1.12 e Å^{-3} and H_b values of −0.87 H Å^{-3}, which is a rather long bond of 1.8592(6) Å, attributed to a zwitterion with a high dipole moment.[52] On the contrary, the S−S bond is not so obvious in a shared interaction, though the BCP is located roughly at the midpoint only 0.03 Å closer to the central S. The electron density at BCP, ρ_b, is 0.6 e Å^{-3}, which is much weaker than that (0.89 e Å^{-3}) of the single bond in L-cystine[5] and that (0.98 e Å^{-3}) in S_7NH and S_8;[20,21] however, the BCP positions are at the midpoint in these compounds. A small positive value of the Laplacian, a small negative H_b value of −0.2 H Å^{-3}, and a value of G_b/ρ_b less than 1 is found in the S−S bond, which could be classified as a shared interaction.[53,54] Furthermore, according to the value of $|V_b|/G_b$, where G_b and V_b are the kinetic and potential energy density, respectively, the bond interaction is classified[53,55] into three categories: a shared interaction with $|V_b|/G_b$ > 2, a transit interaction with $|V_b|/G_b$ = 1−2, and a closed-shell interaction with $|V_b|/G_b$ < 1. Accordingly, the S−S bond is categorized as a transit interaction, i.e., an incipient covalent bond ($|V_b|/G_b$ = 1.51). S−C and C−C are categorized as typical shared interactions, i.e., the covalent bond. In addition, bond paths are located unambiguously between the central S atom and the two terminal S atoms depicted in Figure 6. The location of BCPs manifests that a bond polarization exists along the S−C bond but in much less extent along the S−S bond. A small polarity in S−S bonds is in accord with the 3-center 4-electron (3c−4e) bonding model.[16−18] The ellipticity ($\varepsilon = |\lambda_1/\lambda_2| - 1$) is a measure of the charge distribution from cylindrical symmetry at BCP, the ε value of a typical double bond (ethylene) is 0.45, and that of the conjugated system (benzene) is around 0.23.[56] The ε values of ∼0.2 in the TTP fragment are indicative of a conjugated system. Additional bond delocalization indices, δ(A,B), are calculated by AIMAll[57] and listed in Table 2; the delocalization on the S−C and C−C bonds of the TTP ring is quite obvious. The indices of S(1)−S(2) and S(2)−S(3) are 0.8; however, the index of S(1)···S(3) is 0.2, which indicates the delocalization among S−S−S, thus reinforcing the 3c−4e bonding model. Bond delocalization indices are also applied to the known S−S single-bond system of S_7NH, where the index of the S(1)−S(2) bond is 1.28 but that of S(1)···S(3) is only 0.15; the complete list of δ(A,B) is shown in Figure S5, Supporting Information.

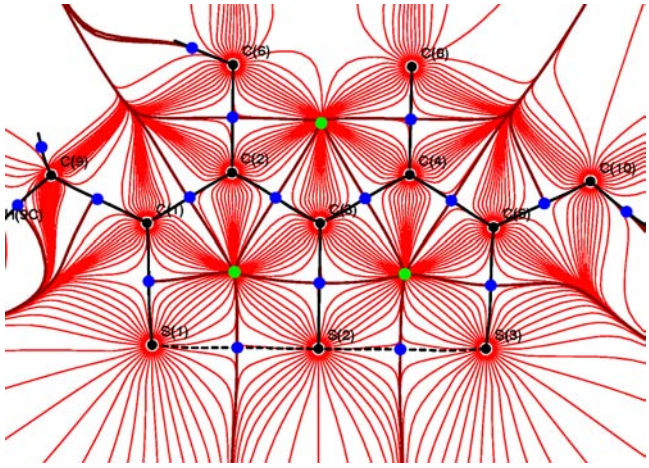

Figure 6. Gradient vector field of electron density at the TTP molecular plane are drawn in red line. Bond paths are in black line. Atomic nuclei or CP (3,−3) are expressed in black dots; BCPs (3,−1) are shown as blue dots, and the ring CP (3,+1) are shown as a green dots.

AIM Charges. The gradient-field trajectory plot at the molecular plane is shown in Figure 6, where the critical points of the atomic nucleus (3, −3) and the ring critical point (3, +1) at the TTP plane are observed from the termination of the trajectories. The atomic basins are obtained from the zero flux surfaces of such trajectory. The atomic basins of sulfur are in a trapezoidal shape with volumes of 25 and 30 Å^3, respectively, for the central and terminal S atoms, shown in Figure S6, Supporting Information. Experimental AIM atomic charges are obtained from integration of the electron density within the atomic basin. The AIM charges and corresponding volume of the atomic basin are listed in Table 3. The volume of C atoms in TTP is ∼10 Å^3 and slightly negative, but that of the substituent is ∼8 Å^3 and slightly positive. The charges of S atoms are negative; however, the central sulfur atom (−0.09e) is lower in charge and smaller in volume (25 Å^3) than those of the terminal ones (−0.38e, 30 Å^3). Of course, the difference in coordination between the central and the terminal S should also be taken into consideration.

Source Function. The source function (SF) is the electron density at any point *r*, $\rho(r)$, partitioned into a sum of atomic contributions within a molecule.[53,58−60] It is a model-independent and qualitative measure of the relative distribution of each atom from the density at any point in a molecule. When the electron density at BCP, ρ_b, is concerned, such partition does provide the information of bond localization or delocalization in the molecule.[61−63] It is similar to the concept in the molecular orbital (MO) calculation, where the electron density from the certain MO can be obtained by the sum of the atomic contributions, which are calculated by the square of the atomic orbital (AO) wave functions multiplied by their coefficients. In addition to bond localization/delocalization, the percentage SF contribution also reflects the bond order as well. For instance, the sum of the percentage SF contributions

dx.doi.org/10.1021/ic4010455 | *Inorg. Chem.* 2013, 52, 10958−10967

Table 3. AIM Atomic Charge (Q) and Volume (V_{001})

	S(1)	S(2)	S(3)	C(1)	C(2)	C(3)	C(6)	C(7)
Q(e)	−0.38	−0.09	−0.38	−0.17	−0.09	−0.10	−0.05	0.03
V_{001}[a]	29.73	25.16	29.83	10.49	10.25	10.39	8.79	8.30

[a] V_{001} is defined as the volume of the region of the atomic basin where $\rho(r)$ is greater than or equal to 0.001 au.

from two bonded C atoms in ρ_b of the C−C bond amounts to 80%, 89%, and 96% in ethane, ethylene, and acetylene, respectively.[61] It is clear that the C−C bond in these molecules is mostly contributed from two bonded C atoms, with the sum of percentage SF contributions increasing with increasing bond order. Both experimental and theoretical data show that the largest individual distribution of the S−S bond is from the two bonded S atoms, as shown in Table 4. The average experimental electron density distributed to the central and terminal S atom from the BCP is 40.2% and 41.4%, respectively. The theoretical SF gives a consistent result with 39.5% and 40.5%, respectively. Similar to the SF analysis of the C−C bond in ethane, the value of ρ_b of the S−S bond is distributed mainly on the two bonded S atoms. A more contracted radial distribution with a higher kappa coefficient (central S:terminal S = 1.03:1.01), smaller atomic basin (25 vs 30 Å^3), and less 'negative AIM charge' (−0.09 vs −0.38e) is found for the central S atom than the terminal one. This is consistent with 3c−4e model in which two electrons in the nonbonding orbital distributes only to the two terminal S atoms. Similarly, the source functions at BCP of the S−C bonds are more than 80% from the bonded atoms; again it distributes more on the S atom than the C atom. S and C is 47% and 35%, respectively, for the central S−C bond and 50% and 37% for the terminal S−C bond. Such feature is in good agreement with the resonance forms indicated in Figure 1.[27,28] In order to see the π delocalization, the SF distributions are investigated when the point of interest is moved 1 au above the TTP plane from the BCP; the main distribution is still on the bonded atoms, listed in Table S2, Supporting Information.

Table 4. Source Function Distributions at BCPs of S−S and S−C of 1

		S(2)−S(1)		S(2)−S(3)	
ρ_b (e/Å^3)	exp	0.607		0.594	
	DFT	0.575		0.561	
atom		ρ (SF) e/Å^3	SF %	ρ (SF) e/Å^3	SF %
S(2)	exp	0.245	40.36	0.238	40.07
	DFT	0.227	39.48	0.220	39.22
S(1)/S(3)	exp	0.251	41.35	0.246	41.41
	DFT	0.233	40.52	0.227	40.46
		S(2)−C(3)		S(1)−C(1)	
ρ_b (e/Å^3)	exp	1.326		1.521	
	DFT	1.386		1.479	
atom		ρ (SF) e/Å^3	SF %	ρ (SF) e/Å^3	SF %
S(2)/S(1)	exp	0.624	47.06	0.753	49.51
	DFT	0.668	48.20	0.779	52.67
C(3)/C(1)	exp	0.466	35.14	0.565	37.15
	DFT	0.492	35.50	0.522	35.29

Fermi Hole (FH) Distribution. According to the molecular structure and topological properties, the S−C and C−C bonds in TTP are all between a single and a double bond, which lead to a bond delocalization in such fragment. The Fermi hole (FH) distribution[64] is based on the Pauli exclusion principle, which represents the probability of finding an electron with the same spin as the reference electron in space; in other words, the distribution correlates exactly with the paired electron spin in space, i.e., an indication of electron localization and delocalization from the reference point. In order to characterize the delocalization of the TTP ring, FH distributions are undertaken cautiously, as depicted in Figures 7 and S7,

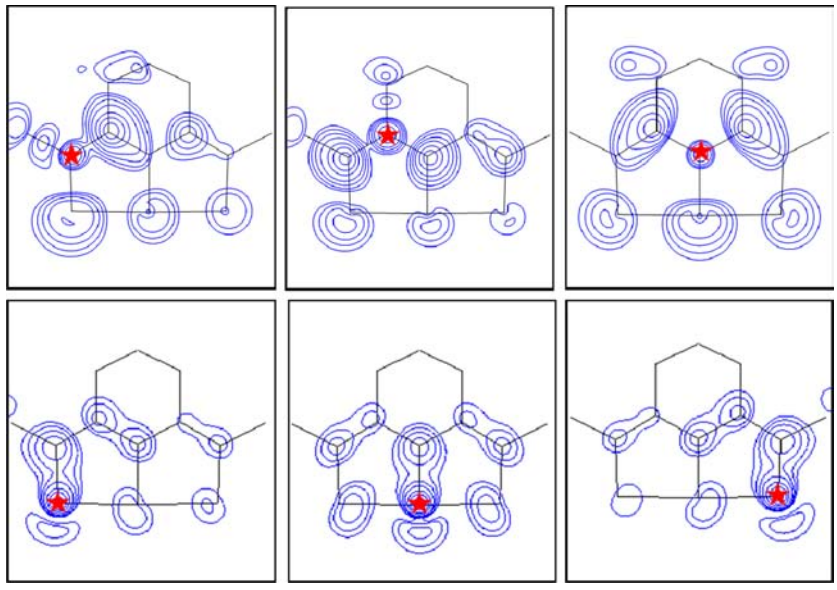

Figure 7. Fermi hole distribution of 2,5-dimethyl-3,4-trimethylene-6a-TTP plotted at the plane 0.7 and 0.9 au above the TTP plane for the top and bottom figures, respectively; reference electron is marked as a red star.

dx.doi.org/10.1021/ic4010455 | Inorg. Chem. 2013, 52, 10958−10967

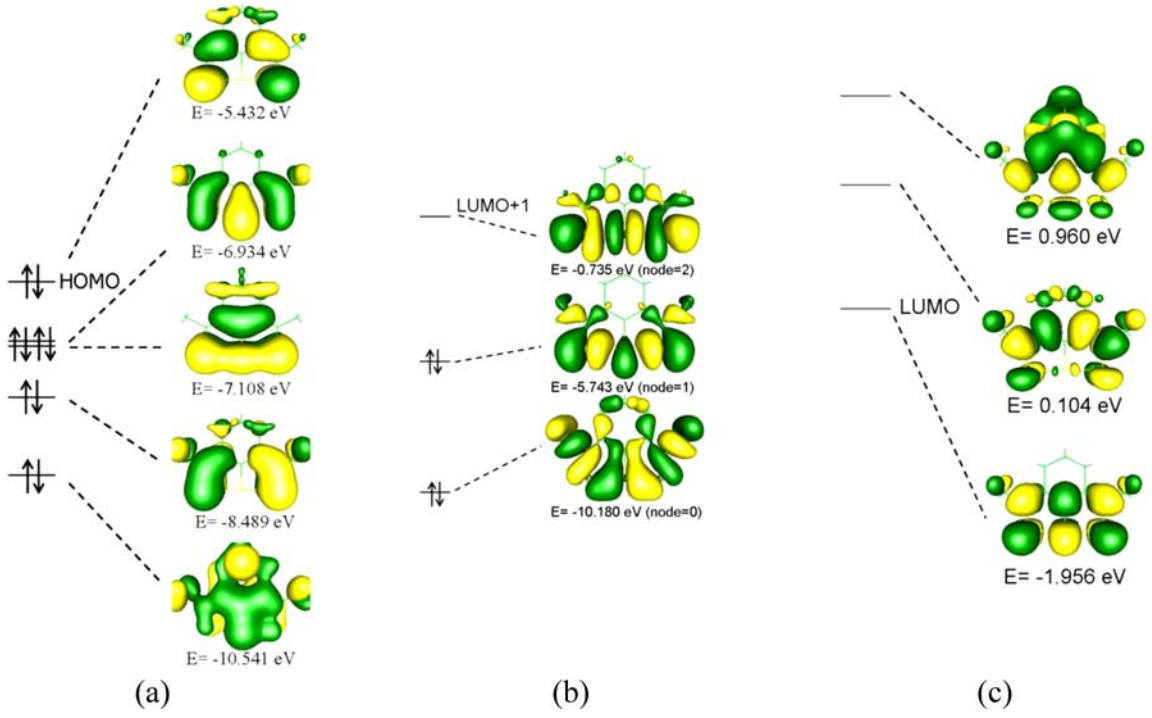

Figure 8. MO diagram of **1**: (a) 10 π electron system (including HOMO), (b) 3c−4e σ bond (σ* orbital (S−S)), and (c) π* orbital (including LUMO).

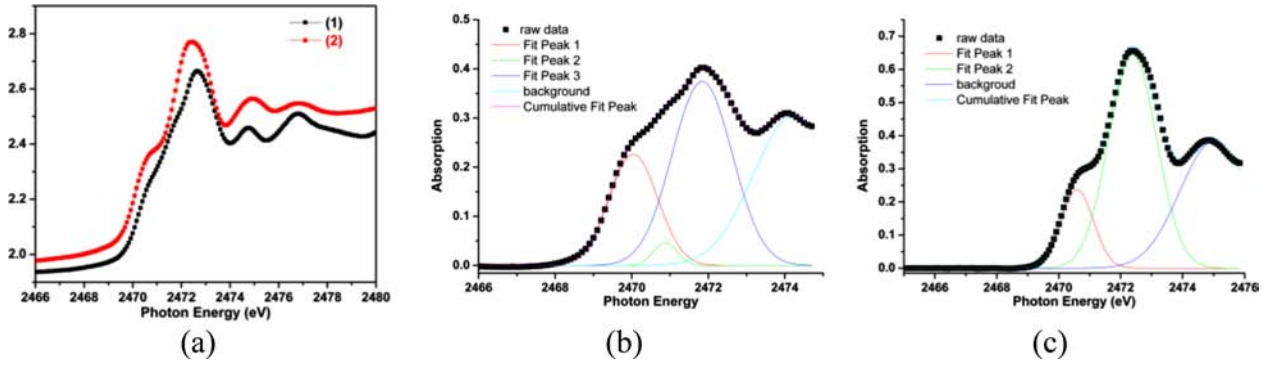

Figure 9. (a) Sulfur K-edge X-ray absorption spectra of **1** and **2**. Profile fitting of the spectra of (b) **1** up to 2475 eV and (c) **2** up to 2476 eV.

Supporting Information; the reference electrons are sequentially placed at 0.9 and 0.7 au above the TTP plane on the S and C atoms in the π directions. With the expected π character, the FH distributions apparently spread out from the selected S and C atoms to the TTP ring of the molecule and the distributions are not extended to the substituents (C(6)−C(10)). It clearly indicates the π delocalization of the TTP ring.

Molecular Orbital Description. All theoretical results mentioned above are derived from a single-point DFT calculation based on the molecular structure obtained by X-ray diffraction at 100 K. They give good agreements with experiment. In order to characterize the chemical bonding from the molecular orbitals, the π orbitals at the TTP ring and the σ orbitals of S−S−S bonds are specially described. There are five occupied π-MOs depicted in Figure 8a, which accommodate 10 π electrons including the highest occupied MO (HOMO), showing the aromatic property. In addition, three σ-MOs mainly along S−S−S bond are shown in Figure 8b, with two MO occupied and one unoccupied (LUMO+1). The 3c−4e bond along S−S−S is thus manifested. Three unoccupied π* orbitals including the lowest unoccupied MO (LUMO) are displayed in Figure 8c. The energy of each corresponding orbital is also given in the figure.

Sulfur K-Edge X-ray Absorption Spectroscopy. Sulfur K-edge XAS is a direct probe to understand the bonding nature concerning the S atom; it is also sensitive to the effective nuclear charge (Z_{eff}). The rising edge energy is normally proportional to Z_{eff}. In other words, the S atom with 'more positive' charge will yield a higher 1s to 3p transition energy. Experimental spectra are depicted in Figure 9a. For comparison purposes, a similar TTP derivative, 2,5-diphenyl-3,4-diaz-6a-TTP (**2**), is also presented. The features in both absorption spectra of **1** and **2** are nearly the same, except at the shoulder region near 2472 eV. After the necessary removal of the higher energy part greater than 2475 eV of **1**, a profile fitting with three peaks is preceded as indicated in Figure 9b; similar treatment is done for **2** and indicated in Figure 9c. TD-DFT-simulated XAS spectra on **1** and **2** are thus fit with the reduced spectra (background subtraction from Figure 9b and 9c); the results are shown in Figure 10a and 10b, respectively. On the

dx.doi.org/10.1021/ic4010455 | Inorg. Chem. 2013, 52, 10958−10967

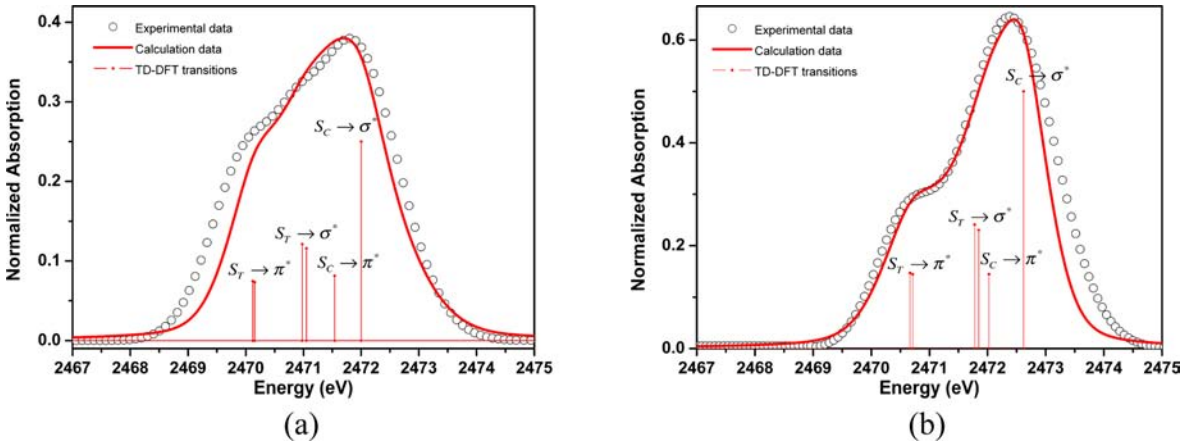

Figure 10. Sulfur K-edge absorption spectra of **1** (a) and **2** (b): reduced experimental (open circle) and TD-DFT calculated (red solid line); calculated transition peaks are displayed as vertical lines.

basis of the calculations, the main absorption peaks are attributed to the S(1s) → π^*(LUMO) and → $\sigma^*_{(S-S-S)}$ (LUMO+1) transitions. Two groups of such transitions are observed: a lower energy group is from the terminal S, and the higher one belongs to the central S. Assignments are indicated in the figure with their energies and relative intensities. As shown in Figure 8c, the LUMO is a π^* character of the TTP ring (with ~13% S_C (p_z), ~24% S_T (p_z), ~15% C_C (p_z), and ~26% C_T (p_z), where subscripts C and T denote the central and terminal atoms, respectively). The LUMO+1 is a σ^* antibonding orbital of the S−S−S bond (with ~28% S_C (p_y), ~32% S_T (p_y), ~0.1% C_C (p), and ~1.3% C_T (p)). The σ^* orbitals of S−C are in the tail part of Figure 10a, namely, the peaks at 2475 and 2477 eV assigned to be the transitions from S(1s) to σ^* orbitals of S−C bonds shown in Figures S9 and S10, Supporting Information, which is removed with the background indicated in Figure 9b. In comparison with the S−C σ^* transition energy of other related compounds, the energy is close to that of *S*-nitroso glutathione (GSNO)[65] (~2474.9 eV) but different from other thiolates, e.g., NaSEt (~2472.1 eV),[65] NaSPh (~2472.9 eV),[65] and CH_3SCH_3(~2472.5 eV).[66,67] In general, the electron-withdrawing phenyl group of S−C(sp^2) will lead to ~0.8 eV higher transition energy than that of the alkyl group of S−C(sp^3) due to the π bonding character. Thus, such transition energy of S−C σ^* may be shifted to even higher energy (~2 eV) if it is involved in a delocalization π-bonding system of ON−S−C bond, such as in the cases of **1**, **2**, and GSNO. This is very similar to the transition energies of S−C σ^* in iron nitrosyl thiolates[43,68,69] or metal dithiolates[70,71] (~2474.5 eV), which are ~1.7 eV higher than those of free ligands.

The π^* orbital (LUMO) energy of **2** is −2.845 eV, which is much lower than that of **1** with −1.956 eV. The lower π^* orbital energy from the terminal S leads to an obvious shoulder peak in **2**. The MO description of **2** is given in Figure S8, Supporting Information. The transition energies from the 1s orbital of the central S atom to the π^*(LUMO) and σ^*(S−S−S) orbitals are evidently higher in energy than those from the terminal S atoms. This again manifests the terminal S atom is more electron rich than the central S atom; this is consistent with the AIM charge from MM refinement. The incipient covalent S−S bond also verifies the 3c−4e bonding model. Besides, the S−S bond distance of **2** is 2.314 Å, about 0.02 Å shorter than that of **1**, which may be attributed to a more stable π system. The UV−vis spectrum is taken for **1**, where two peaks are observed at 489 and 264 nm, which are easily assigned as $\pi \rightarrow \pi^*$ and $\sigma \rightarrow \sigma^*$, respectively, according to the MO description in Figure 8.

CONCLUSION

A combined study of experimental and theoretical charge density together with the sulfur K-edge XAS is carried out on 2,5-dimethyl-3,4-trimethylene-6a-thiathiophthene. The nature of the chemical bond in such a planar TTP ring with a linear S−S−S bond exhibits a 10 π electron aromatic system plus a three-(S)-center four-electron σ bond. The π electrons are evenly distributed among eight atoms (C_5S_3) of TTP. However, the four σ electrons are distributed more at the terminal S atoms than the central one. Therefore, the terminal S atom is relatively more electron rich than the central one, which is in accord with the AIM charge and the sulfur pre-edge absorption position. The bond delocalization indices and source function analyses demonstrate the difference between the central and the terminal S−C bonds. The FH distribution elegantly shows the electron delocalization among the TTP ring atoms.

ASSOCIATED CONTENT

Supporting Information

Additional information on local coordinate setting, residual density map, jnk2RDA residual density analysis, F_o/F_c plot, theoretical 3D Laplacian distribution, delocalization index, atomic basin of central and terminal S atoms, Fermi hole distribution and MO diagram of **2**, comparison of S K-edge spectra of **1** between experiment and TD-DFT calculation, MO diagrams of σ^* of S−C, vertices of VSCC of the S atom and full list of topological properties associated with BCPs of **1**. This material is available free of charge via the Internet at http://pubs.acs.org.

AUTHOR INFORMATION

Corresponding Author

*E-mail: wangyu@ntu.edu.tw.

Notes

The authors declare no competing financial interest.

■ ACKNOWLEDGMENTS

This work was supported by the National Science Council (NSC) and the National Synchrotron Radiation Research Center (NSRRC), Taiwan. Special thanks are due to Dr. Carlo Gatti for providing the software dealing with the source function in the theoretical approach.

■ REFERENCES

(1) Witt, D. *Synthesis* **2008**, 2491−2509.
(2) Kano, N.; Itoh, Y.; Watanabe, Y.; Kusaka, S.; Kawashima, T. *Angew. Chem., Int. Ed.* **2008**, *47*, 9430−9433.
(3) Cremlyn, R. J. *An Introduction to Organosulfur Chemistry*; Wiley: Chichester, 1996.
(4) Sevier, C. S.; Kaiser, C. A. *Nat. Rev. Mol. Cell Biol.* **2002**, *3*, 836−847.
(5) Dahaoui, S.; Pichon-Pesme, V.; Howard, J. A. K.; Lecomte, C. *J. Phys. Chem. A* **1999**, *103*, 6240−6250.
(6) Noury, S.; Silvi, B.; Gillespie, R. J. *Inorg. Chem.* **2002**, *41*, 2164−2172.
(7) Gillespie, R. J.; Silvi, B. *Coord. Chem. Rev.* **2002**, *233*−*234*, 53−62.
(8) Kutzelnigg, W. *Angew. Chem., Int. Ed.* **1984**, *23*, 272−295.
(9) Reed, A. E.; Schleyer, P. v. R. *J. Am. Chem. Soc.* **1990**, *112*, 1434−1445.
(10) Magnusson, E. *J. Am. Chem. Soc.* **1990**, *112*, 7940−7951.
(11) Cioslowski, J.; Mixon, S. T. *Inorg. Chem.* **1993**, *32*, 3209−3216.
(12) Molina, J. M.; Dobado, J. A. *Theor. Chem. Acc.* **2001**, *105*, 328−337.
(13) Grabowsky, S.; Luger, P.; Buschmann, J.; Schneider, T.; Schirmeister, T.; Sobolev, A. N.; Jayatilaka, D. *Angew. Chem., Int. Ed.* **2012**, *51*, 6776−6779.
(14) Schmøkel, M. S.; Cenedese, S.; Overgaard, J.; Jørgensen, M. R. V.; Chen, Y.-S.; Gatti, C.; Stalke, D.; Iversen, B. B. *Inorg. Chem.* **2012**, *51*, 8607−8616.
(15) Leusser, D.; Henn, J.; Kocher, N.; Engels, B.; Stalke, D. *J. Am. Chem. Soc.* **2004**, *126*, 1781−1793.
(16) Hach, R. J.; Rundle, R. E. *J. Am. Chem. Soc.* **1951**, *73*, 4321−4324.
(17) Pimentel, G. C. *J. Chem. Phys.* **1951**, *19*, 446−448.
(18) Musher, J. I. *Angew. Chem., Int. Ed.* **1969**, *8*, 54−68.
(19) Devillanova, F. A. *Handbook of Chalcogen Chemistry: New Perspectives in Sulfur, Selenium and Tellurium*; Royal Society of Chemistry: Cambridge, U.K., 2007.
(20) Lee, C. R.; Tang, T. H.; Chen, L.; Wang, C. C.; Wang, Y. *J. Phys. Chem. Solids* **2004**, *65*, 1957−1966.
(21) Coppens, P.; Yang, Y. W.; Blessing, R. H.; Copper, W. F.; Larsen, F. K. *J. Am. Chem. Soc.* **1977**, *99*, 760−766.
(22) Wang, Y.; Chen, M. J.; Wu, C. H. *Acta Crystallogr., Sect. B* **1988**, *44*, 179−182.
(23) Wang, Y.; Wu, S. Y.; Cheng, A. C. *Acta Crystallogr., Sect. B* **1990**, *46*, 850−854.
(24) Wang, Y.; Yeh, S. K.; Wu, S. Y.; Pai, C. T.; Lee, C. R.; Lin, K. J. *Acta Crystallogr., Sect. B* **1991**, *47*, 298−303.
(25) Lin, K. J.; Wang, Y. *J. Phys. Chem.* **1993**, *97*, 3176−3182.
(26) Hwang, T.-S.; Chong, D. P.; Wang, Y. *J. Chin. Chem. Soc.* **1994**, *41*, 673−677.
(27) Gleiter, R.; Hoffmann, R. *Tetrahedron* **1968**, *24*, 5899−5911.
(28) Pedersen, C. T.; Schaumburg, K. *Org. Magn. Reson.* **1974**, *6*, 586−589.
(29) Bezzi, S.; Mammi, M.; Garbuglio, C. *Nature* **1958**, *182*, 247−248.
(30) Giacometti, G.; Rigatti, G. *J. Chem. Phys.* **1959**, *30*, 1633−1634.
(31) *COLLECT*; Nonius BV: Delft, The Netherlands, 1998.
(32) Duisenberg, A. J. M. EVALCCD, Reflections on area detectors. Ph.D. Thesis, University of Utrecht, 1998.
(33) Sheldrick, G. M. *SADABS*; University of Gottingen: Gottingen, Germany, 1997.
(34) Blessing, R. *J. Appl. Crystallogr.* **1997**, *30*, 421−426.
(35) Clementi, E.; Roetti, C. *At. Data Nucl. Data Tables* **1974**, *14*, 177−478.
(36) Cromer, D. L. *Acta Crystallogr.* **1965**, *18*, 17−23.
(37) Frisch, M. J. *Gaussian 03*, revision D.02; Gaussian, Inc.: Wallingford, CT, 2004.
(38) Ortiz Alba, J. C.; Bo, C. *Xaim-1.0*; Universitat Rovira I Virgili: Tarragona, Spain, 1998; http://www.quimica.urv.es/XAIM.
(39) Volkov, A.; Koritsanszky, T.; Chodkiewicz, M.; King, H. F. *J. Comput. Chem.* **2009**, *30*, 1379−1391.
(40) *OriginPro 9.0*; OriginLab: Northampton, MA.
(41) Neese, F. *ORCA-an ab Initio, Density functional and Semi-empirical Electronic Structure Package*, version 2.9.1; University of Bonn: Germany, 2010.
(42) George, S. D.; Neese, F. *Inorg. Chem.* **2010**, *49*, 1849−1853.
(43) Sun, N.; Liu, L. V.; Dey, A.; Villar-Acevedo, G.; Kovacs, J. A.; Darensbourg, M. Y.; Hodgson, K. O.; Hedman, B.; Solomon, E. I. *Inorg. Chem.* **2011**, *50*, 427−436.
(44) Sarangi, R.; Yang, L.; Winikoff, S. G.; Gagliardi, L.; Cramer, C. J.; Tolman, W. B.; Solomon, E. I. *J. Am. Chem. Soc.* **2011**, *133*, 17180−17191.
(45) Johnson, P. L.; Llaguno, E. C.; Paul, I. C. *J. Chem. Soc., Perkin Trans. 2* **1976**, 234−238.
(46) Hansen, N. K.; Coppens, P. *Acta Crystallogr., Sect. A* **1978**, *34*, 909−921.
(47) Coppens, P. *X-Ray Charge Densities and Chemical Bonding*; Oxford University Press: Oxford, 1997.
(48) Volkov, T.; Macchi, P.; Farrugia, L. J.; Gatti, C.; Mallinson, P.; Richter, T.; Koritsanszky, T. *XD2006-A computer program for multipole refinement, topological analysis of charge densities, evaluation of intermolecular energies from experimental or theoretical structure factors*; University of Buffalo, Buffalo, NY, 2006.
(49) Meindl, K.; Henn, J. *Acta Crystallogr., Sect. A* **2008**, *64*, 404−418.
(50) Fischer, A.; Tiana, D.; Scherer, W.; Batke, K.; Eickerling, G.; Svendsen, H.; Bindzus, N.; Iversen, B. B. *J. Phys. Chem. A* **2011**, *115*, 13061−13071.
(51) Koritsanszky, T. S.; Coppens, P. *Chem. Rev.* **2001**, *101*, 1583−1628.
(52) Lee, C.-R.; Tang, T.-H.; Chen, L.; Wang, Y. *Chem.—Eur. J.* **2003**, *9*, 3112−3121.
(53) Gatti, C. *Z. Kristallogr.* **2005**, *220*, 399−457.
(54) Macchi, P.; Sironi, A. *Coord. Chem. Rev.* **2003**, *238*−*239*, 383−412.
(55) Espinosa, E.; Alkorta, I.; Elguero, J.; Molins, E. *J. Chem. Phys.* **2002**, *117*, 5529−5542.
(56) Bader, R. F. W.; Slee, T. S.; Cremer, D.; Kraka, E. *J. Am. Chem. Soc.* **1983**, *105*, 5061−5068.
(57) Keith, T. A. *AIMAll* (Version 13.05.06); TK Gristmill Software: Overland Park, KS, 2013; aim.tkgristmill.com.
(58) Bader, R. F. W.; Gatti, C. *Chem. Phys. Lett.* **1998**, *287*, 233−238.
(59) Gatti, C.; Cargnoni, F.; Bertini, L. *J. Comput. Chem.* **2003**, *24*, 422−436.
(60) Farrugia, L. J.; Macchi, P. *J. Phys. Chem. A* **2009**, *113*, 10058−10067.
(61) Gatti, C.; Lasi, D. *Faraday Discuss.* **2007**, *135*, 55−78.
(62) Gatti, C.; Bertini, L. *Acta Crystallogr., Sect. A* **2004**, *60*, 438−449.
(63) Lo Presti, L.; Gatti, C. *Chem. Phys. Lett.* **2009**, *476*, 308−316.
(64) Bader, R. F. W. *Atoms in Molecules—A Quantum Theory*; Oxford University Press: New York, 1990.
(65) Szilagyi, R. K.; Schwab, D. E. *Biochem. Biophys. Res. Commun.* **2005**, *330*, 60−64.
(66) Pickering, I. J.; Prince, R. C.; Divers, T.; George, G. N. *FEBS Lett.* **1998**, *441*, 11−14.
(67) Hitchcock, A. P.; Bodeur, S.; Tronc, M. *Physica B* **1989**, *158*, 257−258.
(68) Lu, T. T.; Lai, S. H.; Li, Y. W.; Hsu, I. J.; Jang, L. Y.; Lee, J. F.; Chen, I. C.; Liaw, W. F. *Inorg. Chem.* **2011**, *50*, 5396−5406.
(69) Yeh, S. W.; Lin, C. W.; Li, Y. W.; Hsu, I. J.; Chen, C. H.; Jang, L. Y.; Lee, J. F.; Liaw, W. F. *Inorg. Chem.* **2012**, *51*, 4076−4087.

(70) Solomon, E. I.; Hedman, B.; Hodgson, K. O.; Dey, A.; Szilagyi, R. K. *Coord. Chem. Rev.* **2005**, *249*, 97−129.
(71) Sarangi, R.; DeBeer George, S.; Rudd, D. J.; Szilagyi, R. K.; Ribas, X.; Rovira, C.; Almeida, M.; Hodgson, K. O.; Hedman, B.; Solomon, E. I. *J. Am. Chem. Soc.* **2007**, *129*, 2316−2326.